Electronic Supplementary Material (ESI) for Green Chemistry.

# Supporting Information

## An ultimate anode renders protic ionic liquids sustainability in metal electrodeposition

**Yi-Ting Chen, [a] Hsing-Yin Chen, [a] Yu-Shan Chien, [a] Min-Chieh Chuang, [*b] Po-Yu Chen, [*acd]**

[a]*Department of Medicinal and Applied Chemistry, Kaohsiung Medical University, Kaohsiung, Taiwan ROC*
[b]*Department of Chemistry, Tunghai University, Taichung, Taiwan ROC*
[c]*Department of Medical Research, Kaohsiung Medical University Hospital, Kaohsiung, Taiwan ROC*
[d]*Department of Chemistry, National Sun Yat-sen University, Kaohsiung, Taiwan ROC*

## Table of contents

## 1. Experimental procedures

### *Chemicals, apparatuses, and electrochemical experiments*

All chemicals were used as received without further purification except that copper wire (diameter: 1 mm, 99.9%, Alfa Aesar), lead plate (thickness: 1 mm, 99.998%, Alfa Aesar) and platinum wire (diameter 0.5 mm, 99.95%, Alfa Aesar) were cleaned by soaking in acetone, diluted nitric acid, and doubly-deionized water (Resistance > 18 MΩ $cm^{-1}$; supplied by a Millipore Smart Simplicity System) in sequence, and then dried under ambient air before using them. The hydrophobic protic ionic liquid (IL) [Hbet][TFSA] was synthesized by following the procedures previously reported.[1,2] In brief, betaine hydrochloride ([Hbet][Cl], ≥99%, Sigma-Aldrich) and lithium bis((trifluromethyl)sulfonyl)amide ([Li][TFSA], >98%, 3M) were mixed in equal moles in an appropriate amount of water, and then stirred using a magnetic stirrer until two transparent layers of liquid were observed. The upper layer was water solution containing LiCl and the bottom layer was the IL [Hbet][TFSA]. The latter was washed with iced water for several times until no precipitates could be observed after introducing $AgNO_3$ solution to the aqueous phase. The obtained transparent [Hbet][TFSA] was dried by vacuum using an oil pump at 120°C for at least one day. The melting point of [Hbet][TFSA] is ca. 57°C. Therefore, it became a white solid after cooling it down, and then stored in the nitrogen-filled glove box (PL-HE-10-404, Innovative Technology). The chemical structure of [Hbet][TFSA] can be found in Fig. S1. [Hbet] (cation of the IL) can deprotonate to produce the zwitterion [bet]. The hydrophilic protic IL [MeIm][Ac] was prepared in accordance with the procedures reported in the literature.[3,4]

All electrochemical experiments were conducted at 40°C in a traditional one-compartment three-electrode electrochemical cell in which the reference electrode was a $Ag/AgCl_{IL}$[5] (the electrode potential was thus reported with respect to this electrode (vs. $Ag/AgCl_{IL}$)), working electrode is glassy carbon disc electrode (GCE, diameter: 3 mm, No. 002012, ALS Co., Ltd), platinum disc electrode (PtE, diameter: 1.6 mm, MF-2013, Bioanalytical System (BAS)), copper disk electrode (CuE, diameter: 3 mm, No. 012587, ALS Co., Ltd), Cu coil (made from copper wire) or Pb plate, and counter electrode was Pt coil (made from platinum wire), unmodified carbon rod electrode (unmodified CRE), IrOx-functionalized CRE (CRE\IrOx), or IrOx-functionalized Pt coil (Pt\IrOx). A porosity E glass frit (ACE Glass Inc.) was used for the counter electrode to separate it from the bulk solution if being required. The electrochemical cell was controlled by a CHI 440A or 760C electrochemical analyzer (CH Instruments, Inc.) for voltammetric study and bulk electrodeposition of metals. The cell contained [Hbet][TFSA] or [MeIm][Ac] with 9 wt% $H_2O$ ([Hbet][TFSA]/$H_2O$ or

[MeIm][Ac]/$H_2O$) as the electrolytes, and 1 wt% PbO (>99%, Merck), 4.0 wt% ZnO (>99%, Merck), or 0.5 wt% CuO (Extra pure, Santoku Chemical), was introduced to prepare a transparent Pb(II), Zn(II) (only [Hbet][TFSA] was used for preparing Zn(II) solution), or blue Cu(II) solution. Cyclic voltammetry was performed under a potential scan rate of 50 $mVs^{-1}$, and bulk electrodeposition was conducted potentiostatically at −0.4 V, −0.3 V, and −1.0 V, respectively, for Pb, Cu, and Zn in [Hbet][TFSA]/$H_2O$ but −0.7 V and −0.9 V, respectively, for Cu and Pb in [MeIm][Ac]/$H_2O$. The number of the accumulated charge during the bulk electrodeposition was recorded ($Q_{exp}$). The metal electrodeposits were soaked in neat ethanol twice to remove the residual IL, dried under nitrogen, and weighed to get the net weight of metal deposits ($\Delta m_{exp}$) using an electronic balance precise to 0.1 mg. After the accomplishment of bulk electrodeposition, water was introduced to the electrolyte until an identical anodic limit of potential as similar as the original one was observed (see Fig. 3a). PbO or CuO was reloaded to the electrolyte based on the $\Delta m_{exp}$ measured in the last round of bulk electrodeposition, and the corresponding CV (as shown in Fig. 3b and Fig. S3 for examples) was recorded. Afterwards, the next round of bulk electrodeposition was carried out.

### *Preparation of IrOx electrode*

*Synthesis of Ir-precursor.*—Synthesis of a solution containing $[Ir(OH)_6]^{2-}$ was performed as previously.[6,7] Briefly, 33 mg $K_2IrCl_6$ was dissolved in ultrapure $H_2O$ (32.5 mL) under stirring at ambient temperature for 1 hour. Aliquots (2.17 mL) of NaOH solution (10 wt%) was added dropwise into the solution, which was subsequently held at 95°C for 20 min under agitation. Immediately the resultant solution was cooled in an ice bath for 1 hour and stored at 4°C for at least 24 hours before any experimental use.

*Electroflocculation.*—Deposition of IrOx on CRE or Pt coil was conducted in the electrochemical cell containing the CRE (or Pt coil), a Pt plate, and a saturated calomel electrode (SCE) as working, counter, and reference electrodes, respectively. A technique − dual-potential pulsed amperometry, whereby 1.3 and −0.7 V were applied intermittently (1-s pulse period for each potential), was performed in a 0.525 mM $[Ir(OH)_6]^{2-}$ solution for total deposition time in 20 min. The resulting CRE\IrOx or Pt\IrOx was subsequently rinsed with ultrapure $H_2O$ thoroughly.

### *Computation*

The present density functional theory (DFT) calculations were carried out at B3LYP/6-31+G(d) level. The Grimme's D3 dispersion correction with Becke-Johnson damping[8] was added to improve the description of weak intermolecular interactions. The SMD continuum solvation model[9] with a dielectric constant $\varepsilon = 10$ was used to mimic the ionic liquid environment. This $\varepsilon$ value was selected as the dielectric constant of room-temperature ionic liquids falls in the range of 9−15.[10,11] The setting of ultrafine grid was adopted for numerical integration. Thermal correction to Gibbs free energy was performed at the standard conditions of 298.15 K and 1 atm. All calculations were accomplished by using Gaussian 09 package.[12]

## 2. Supplementary experimental data

### *NMR analysis of upper transparent IL*

As indicated in the main text, the electrolyte turned dark if IrOx-functionalized electrode is not used as anode for the bulk electrodeposition of Pb. The darkened electrolyte was stand still for a sufficient period to permit the dark species precipitate. $^{13}$C and $^{19}$F NMR spectra of the transparent upper layer (Fig. 2e) were recorded by using deuterated methanol as the solvent, and the spectra are shown in Fig. S1.

Fig. S1 indicates that the IL in the transparent layer after the bulk electrolysis still owned the same chemical structures as the fresh IL. It was thus supposed that IL was not damaged by the dark species, and no detectable new species existed in the upper layer. However, IL was definitely continuously decomposed if the bulk electrolysis is lasted.

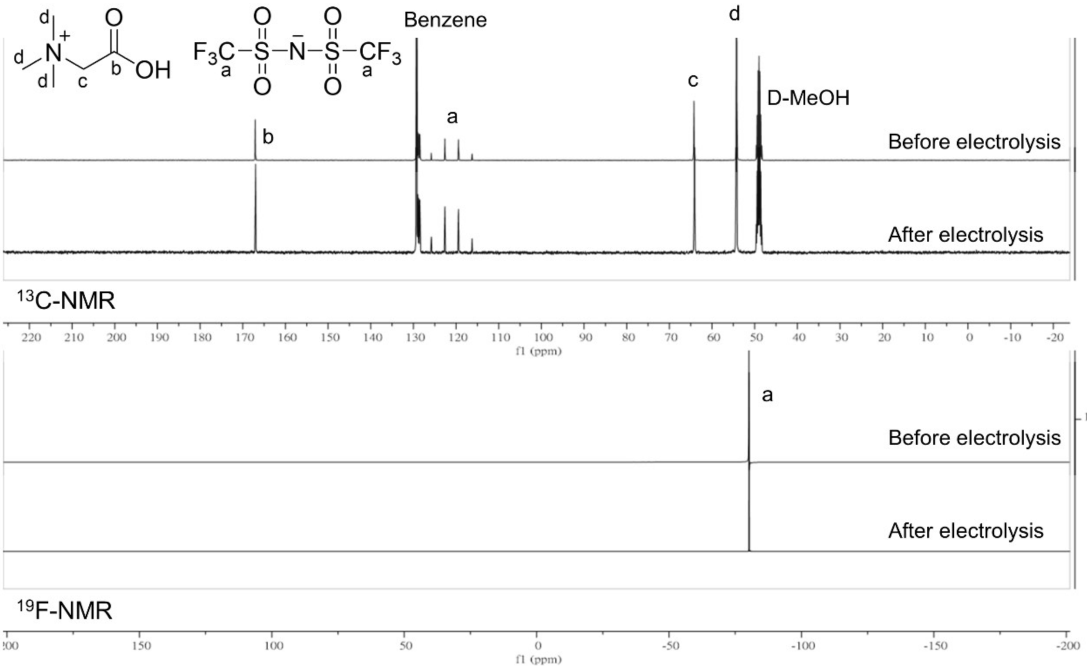

Fig. S1 $^{13}$C- and $^{19}$F-NMR spectra of the transparent upper layer (the photo of the upper layer is shown in Fig. 2e).

### *EDX, Raman, and FT-IR analysis of the dark precipitates*

The dark precipitates were collected by centrifugation, the supernatant IL was removed, and an appropriate amount of fresh ethanol was introduced to disperse and wash the precipitates in an eppendorf tube. The abovementioned procedures were repeated for at least five times to remove the residual IL, and then the dark precipitates were dried in a vacuum oven for the following chemical identification. Energy dispersive X-ray spectrum (EDX) shows that the precipitates were majorly composed of C and O accompanied with traced Pb (Fig. S2a). It was supposed that Pb was not the fundamental component of the precipitates but adsorbed on them. Raman spectra indicated that no graphite structure could be detected (data are not shown; only noises were recorded). The FI-IR spectra of the discs prepared by mixing KBr and the dark precipitates, [Hbet][Cl] (cation of the IL), or [Li][TFSA] (anion of the IL) are shown in Fig. S2b. As can be seen, the precipitates showed no characteristic vibrational signals as the cation and anion of the IL, respectively. Taking all above together, the precipitates were probably the fragments of the cations electrochemically decomposed at the anode during the bulk electrodeposition. The precipitates showed typical signals of C−H stretching (2961, 2925, and 2853 $\text{cm}^{-1}$), C−O stretching of alcohol (1181, 1142 $\text{cm}^{-1}$), C−O stretching of ether (1075 $\text{cm}^{-1}$), O−H stretching (3449 $\text{cm}^{-1}$), and C−H bending (834 $\text{cm}^{-1}$). The detailed chemical structures and the formation mechanism of the precipitates need to be further resolved in the future.

It needs to emphasize that the IR spectra of our protonated-betaine chloride (betaine hydrochloride; [Hbet][Cl]) and lithium bis((trifluoromethyl)sulfonyl)amide ([Li][TFSA]) are similar to the data shown in the database and a previous paper,[13,14] respectively.

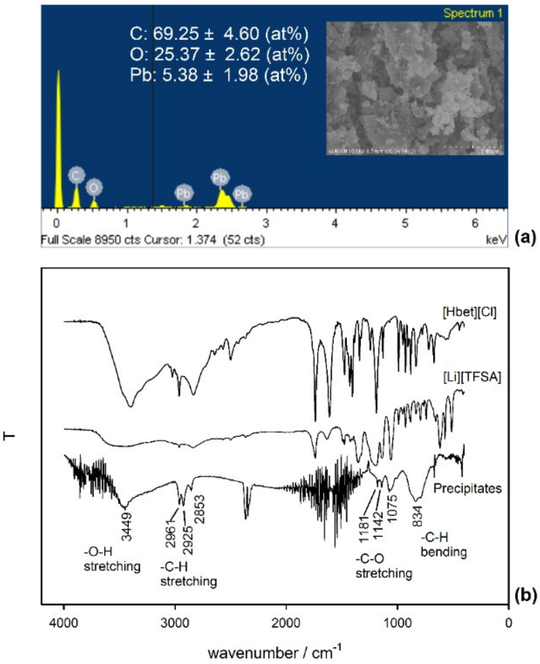

Fig. S2 (a) EDX analysis and SEM image of the dark precipitates. (b) FT-IR spectra of the indicated species.

### *CVs of Cu(II) and Zn(II) before and after bulk electrolysis*

As Fig. 3b shows, the CVs were recorded before and after the bulk electrolysis of metals. Before the next round of electrodeposition was conducted, an appropriate amount of water and the metal oxide (metal oxide was introduced based on how much was consumed in the previous round of bulk electrolysis) were introduced to refresh the solutions. However, this procedure was not used for Zn electrodeposition because a relatively negligible amount of ZnO was consumed during the bulk electrodeposition. The CVs recorded before and after the bulk electrolysis, and after the solution was refreshed are shown in Fig. S3.

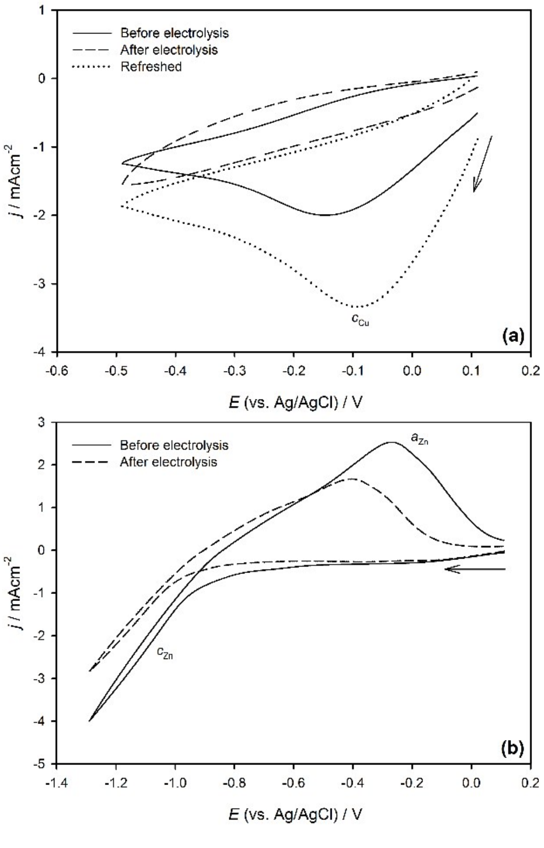

Fig. S3. CVs recorded at CuE in [Hbet][TFSA]/$H_2O$ containing (a) CuO and (b) ZnO, respectively.

After the solution was refreshed, the reductive wave of Cu(II) + $2e^{-} \rightarrow$ Cu was apparently bigger than that recorded before electrolysis because a little bit excess water was introduced in the refreshing step.

## CVs of Cu(II) in [Hbet][TFSA]/$H_2O$ and in [MeIm][Ac]/$H_2O$, respectively

The CVs recorded at CuE in [Hbet][TFSA]/$H_2O$ and [MeIm][Ac]/$H_2O$, respectively, containing CuO are shown in Fig. S4. $c_{\mathrm{Cu}}$ and $a_{\mathrm{Cu}}$ are reductive and oxidative waves, respectively, for the reaction Cu(II) + $2e^-$ ⇌ Cu. $a_{\mathrm{Cu}}$ wave was not observed in [Hbet][TFSA]/$H_2O$ because the potential was not scanned to where Cu was oxidized in order to prevent oxidation of CuE. In [MeIm][Ac]/$H_2O$, the potential was scanned to where Cu was oxidized in order to make the redox couple $c_{\mathrm{Cu}}/a_{\mathrm{Cu}}$ more apparent. As can be seen, Cu(II) needed a higher overpotential to be reduced to Cu in [MeIm][Ac]/$H_2O$, implying that Cu(II) should be more easily oxidized in this electrolyte.

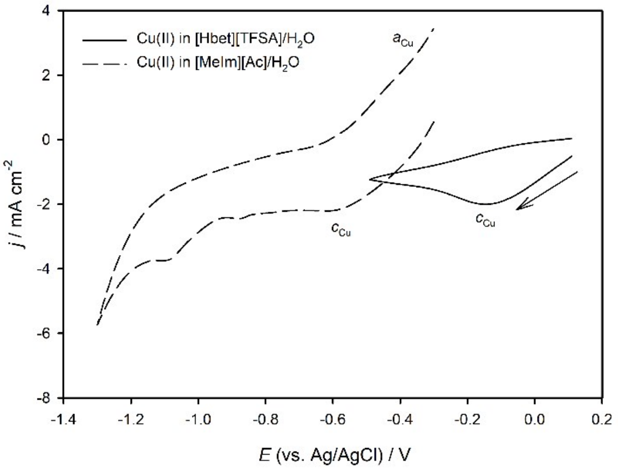

Fig. S4. CVs recorded at CuE in [Hbet][TFSA]/$H_2O$ and [MeIm][Ac]/$H_2O$, respectively, containing CuO.

## Computational results

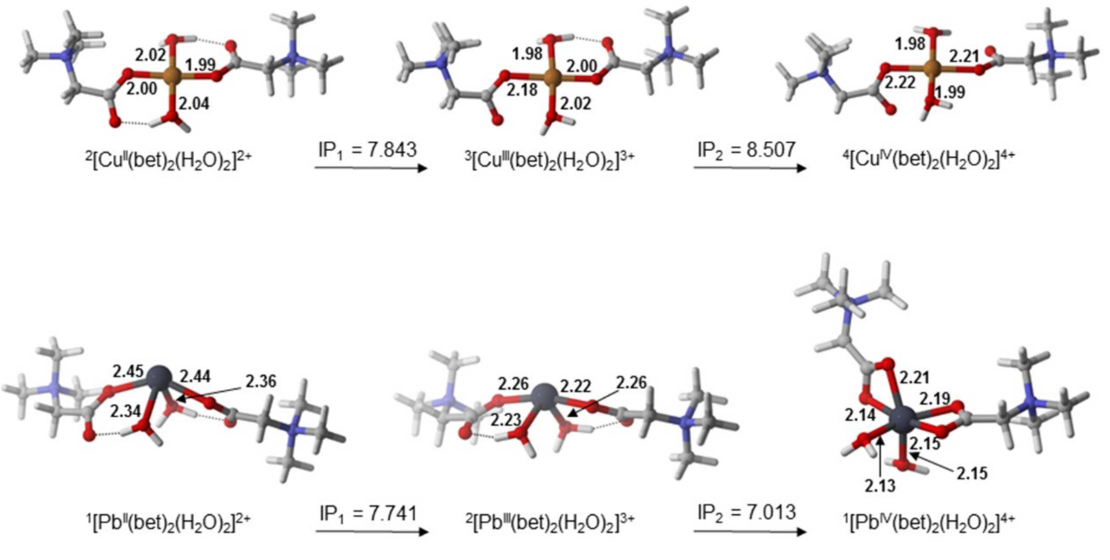

Fig. S5. DFT optimized structures and ionization potentials (eV) of Cu and Pb complexes in

[Hbet][TFSA]/$H_2O$ mixture.

The first ($IP_1$) and the second ionization potentials ($IP_2$) of $[Cu(bet)_2(H_2O)_2]^{2+}$ and $[Pb(bet)_2(H_2O)_2]^{2+}$ were calculated to shed some light on the oxidation behavior of Cu(II) and Pb(II) species in [Hbet][TFSA]/$H_2O$ mixture. The theoretical IPs and the optimized structures are shown in Fig. S5. The calculations revealed that the $[Cu(bet)_2(H_2O)_2]^{2+}$ formed a square planar geometry in which the [bet] ion coordinates to the Cu(II) through one of the oxygen atoms of carboxylate group. Upon ionization the coordination bond distances between Cu and ligands varied but the geometry remained unchanged. In contrast, the $[Pb(bet)_2(H_2O)_2]^{2+}$ and $[Pb(bet)_2(H_2O)_2]^{3+}$ displayed a distorted seesaw structure and then changed to a distorted octahedral structure upon second ionization. In addition, it was found that the $IP_2$ (7.013 eV) was smaller than the $IP_1$ (7.741 eV) for $[Pb(bet)_2(H_2O)_2]^{2+}$, implying that this species will undergo two-electron oxidation. Also, the ionization potentials of $[Pb(bet)_2(H_2O)_2]^{2+}$ were smaller than those of $[Cu(bet)_2(H_2O)_2]^{2+}$ ($IP_1$ = 7.843 eV and $IP_2$ = 8.507 eV). These computational results suggest that the Pb(II) species is more easily oxidized compared to the Cu(II) species in [Hbet][TFSA].

## References

1. P. Nockemann, B. Thijs, S. Pittois, J. Thoen, C. Glorieux, K. Van Hecke, L. Van Meervelt, B. Kirchner, K. Binnemans, Task-specific ionic liquid for solubilizing metal oxides, *Journal of Physical Chemistry B* 110 (2006) 20978-20992.
2. H.-W. Yeh, Y.-H. Tang, P.-Y. Chen, Electrochemical study and extraction of Pb metal from Pb oxides and Pb sulfate using hydrophobic Brønsted acidic amide-type ionic liquid: a feasibility demonstration, *Journal of Electroanalytical Chemistry* 811 (2018) 68-77.
3. D. R. MacFarlane, J. M. Pringle, K. M. Johansson, S. A. Forsyth, M. Forsyth, Lewis base ionic liquids, *Chemical Communications* (2006) 1905-1917.
4. T. L. Greaves, C. J. Drummond, Protic ionic liquids: properties and applications, *Chemical Reviews* 108 (2008) 206-237.
5. N.-C. Lo, P.-C. Chung, W.-J. Chuang, S.C.N. Hsu, I-W. Sun, P.-Y. Chen, Voltammetric study and electrodeposition of Ni(II)/Fe(II) in the ionic liquid 1-butyl-1-methylpyrrolidinium dicyanamide, *Journal of The Electrochemical Society* 163 (2016) D9-D16.
6. P.-Y. Liu, C.-C. Hsu, M.-C. Chuang, Hemin-mediated construction of iridium oxide with superior stability for the oxygen evolution reaction, *Journal of Materials Chemistry A* 5 (2017) 2959-2971.
7. P.-Y. Liu, S.-C. Sun, Y.-S. Chen, M.-C. Chuang, Efficient electrocatalytic reduction and detection of hydrogen peroxide at an Ir(IV)Ox·$H_2O$ nanostructured

electrode prepared by electroflocculation, *Electrochimica Acta* 187 (2016) 256-263.

8. S. Grimme, S. Ehrlich, L. Goerigk, Effect of the damping function in dispersion corrected density functional theory, *Journal of Computational Chem*istry 32 (2011) 1456-1465.
9. A. V. Marenich, C. J. Cramer, D. G. Truhlar, Universal solvation model based on solute electron density and a continuum model of the solvent defined by the bulk dielectric constant and atomic surface tensions, *Journal of Physical Chemistry B* 113 (2009) 6378-6396.
10. F. Dommert, J. Schmidt, B. Qiao, Y. Zhao, C. Krekeler, L.D. Site, R. Berger, C. A. Holm, Comparative study of two classical force fields on static and dynamics of [EMIM][$BF_4$] investigated via molecular dynamics simulations, *Journal of Chemical Physics* 129 (2008) 224501-224510.
11. C. Wakai, A. Oleinikova, M. Ott, H. Weingärtner, How polar are ionic liquids? Determination of the static dielectric constant of an imidazolium-based ionic liquid by microwave dielectric spectroscopy, *Journal of Physical Chemistry B* 109 (2005) 17028-17030.
12. M. J. Frisch, G. W. Trucks, H. B. Schlegel, G. E. Scuseria, M. A. Robb, J. R. Cheeseman, G. Scalmani, V. Barone, B. Mennucci, G. A. Petersson, G. A. et al. Gaussian 09, revision A.02; Gaussian, Inc.: Wallingford, CT, 2009.
13. NIST Chemistry WebBook. https://webbook.nist.gov/cgi/cbook.cgi?Name=Betaine+hydrochloride&Units=SI
14. J. Cardoso, A. Mayrén, I. C. Romero-Ibarra, D. P. Nava, J. Vazquez-Arenas, Nanocomposite polymer electrolytes based on poly(poly(ethylene glycol)methacrylate), MMT or ZSM-5 formulated with LiTFSI and PYR11TFSI for Li-ion batteries, *RSC Advances* 6 (2016) 7249-7259.